International Journal of Solids and Structures 54 (2015) 20–30

Contents lists available at ScienceDirect

International Journal of Solids and Structures

journal homepage: www.elsevier.com/locate/ijsolstr

Structural templates of disordered granular media

David M. Walker [a], Antoinette Tordesillas [a,b,*], Jie Zhang [d], Robert P. Behringer [e], Edward Andò [f], Gioacchino Viggiani [g], Andrew Druckrey [c], Khalid Alshibli [c]

[a] Department of Mathematics & Statistics, University of Melbourne, Parkville, VIC 3010, Australia
[b] School of Earth Sciences, University of Melbourne, VIC 3010, Australia
[c] Department of Civil and Environmental Engineering, University of Tennessee, Knoxville, TN 37996, USA
[d] Department of Physics and Astronomy, Shanghai Jiao Tong University, China
[e] Department of Physics, Duke University, Durham, NC 27708, USA
[f] CNRS, 3SR, F-38000 Grenoble, France
[g] Univ.Grenoble Alpes, 3SR, F-38000 Grenoble, France

ARTICLE INFO

Article history:
Received 18 September 2014
Received in revised form 27 October 2014
Available online 23 November 2014

Keywords:
Complex networks
Motifs
Granular materials

ABSTRACT

Granular materials, in common with many complex systems, exhibit a range of self-organization processes that control their mechanical performance. Many of these processes directly manifest in the evolution of the contact network as the material responds to applied stresses and strains. Yet the connections between the topology, structure and dynamics of this evolving contact network remain poorly understood. Here we demonstrate that dense granular systems under a variety of loading conditions exhibit preferred structural ordering reminiscent of a superfamily classification. In particular, two distinct superfamilies are discovered: the first is typically exhibited by materials in the pre-failure regime, while the second manifests in the unstable or failure regime. We demonstrate the robustness of these findings with respect to a range of packing fractions in experimental sand and photoelastic disk assemblies subject to compression and shear, as well as in a series of discrete element simulations of compression tests. We show that the superfamily classification of small connected subgraphs in a granular material can be used to map boundaries in a so-called jamming phase diagram and, consequently, offers a key opportunity to bridge the mechanics and physics perspectives on the constitutive behavior of granular systems.

1. Introduction

The development of predictive continuum models for granular materials has a long history. A missing ingredient in this effort in the period preceding the introduction of high-resolution or grain-scale measurements, is knowledge of the *evolving internal structure* in the course of deformation of the material. Despite recent collection of grain-scale measurements, explicit information on the dominant structures, their most pervasive topologies or fabric, and their dynamics are surprisingly lacking. We know of only one system where this information has been comprehensively established and this is based on data from a physical experiment in two dimensions (Tordesillas et al., 2012).

Here we combine the concepts of network motifs pioneered by Milo et al. (2002) and the superfamily phenomenon of Xu et al. (2008) to study the defining fabric of dense granular materials. We study a total of nine tests from simulations and experiments involving two-dimensional and three-dimensional granular materials subjected to different loading tests. The two-dimensional data sets from simulations comprise two biaxial compression tests subject to constant volume boundary conditions (see, for example, Tordesillas, 2007). In three-dimensions, the data from simulations include a compression test of an assembly of polyellipsoidal particles (Peters et al., 2009); a sample of spheres constrained to follow a proportional strain loading path to induce diffuse failure (Sibille et al., 2009); and a sample of spheres subject to shear to study permeability within dilatant shear bands (Sun et al., 2013). Three experimental three-dimensional triaxial tests are considered where μ-CT X-ray methods allow identification of grains and their contacts. Two sand types, Caicos ooid and Hostun, are examined using data from Andò et al. (2013). A third sand type, Ottawa, is examined using data from Druckrey and Alshibli (2014). Some of the samples fail by strain localization, while others exhibit diffuse failure. In addition to these, we also characterize a unique series of

* Corresponding author at: Department of Mathematics & Statistics, University of Melbourne, Parkville, VIC 3010, Australia.
E-mail address: atordesi@unimelb.edu.au (A. Tordesillas).

http://dx.doi.org/10.1016/j.ijsolstr.2014.11.013
0020-7683/

90 experimental runs that were conceived to explore a recently postulated phase diagram where photoelastic disk assemblies across a range of packing fractions were sheared until they become shear-jammed, i.e., there is a percolating strong network in both spatial directions (Bi et al., 2011). The question we seek to address is: *With respect to structure and structural evolution, is there an unambiguous structural property common to these systems despite the difference in dimensionality, loading condition, material or failure mode?*

To place this effort more precisely with respect to the state of knowledge, not just in the physics and mechanics of granular materials, but also the mathematics and statistics of complex systems, we briefly review some pertinent advances across these disciplines. Broadly, our strategy is to characterize the structure and functionality of each system by mapping material properties to a complex network (Walker and Tordesillas, 2010). By far the most studied is the contact network, although other complex networks based on kinematics and other properties besides the contacts also prove useful. The study of the complex network properties permits the quantitative characterization of structural evolution in an entirely multiscale framework. In many cases, the structure can be characterized using macroscopic quantities which are typically global averages of local microscopic quantities across the entire network (Walker and Tordesillas, 2010). That said, the functionality that is critical to macroscopic granular behavior manifests itself, not at the grain-scale, but at the mesoscale where emergent patterns (e.g., force chains, vortices etc.) and instabilities are the norm. Thus, in the past, much effort has been devoted to the intermediate mesoscopic scale: here structural properties of networks have been investigated, including the prevalence of contact cycles of a given length scale (Tordesillas et al., 2010; Arévalo et al., 2010), the population and transition dynamics of small subgraphs (Tordesillas et al., 2012), assortativity patterns of pore connectivity (Russell et al., submitted for publication), the characteristic length scales of network communities (Tordesillas et al., 2013), to name a few. Recently, Matsushima and Blumenfeld (2014) have uncovered some universal emergent structural properties of 2D granular packings seemingly independent of some material properties within their quadron formulation.

In this study, we are interested in the topology of mesoscopic structures in the contact network which consist of the set of connected subgraphs with four vertices and associated edges (see, Fig. 1 where the subgraphs are itemized by A, B, C, D, E and F). We consider four rather than three vertex subgraphs because in an undirected network there are only two such three vertex subgraphs, namely, a closed and an open triangle; on the other hand, five or higher number vertex subgraphs are challenging to enumerate and their identification in a general network remain a difficult problem. Although it is a challenge to identify the exact number of all six possible four vertex subgraphs in a network, algorithms do exist for determining these tetrad structures (e.g., Kashani et al., 2009).

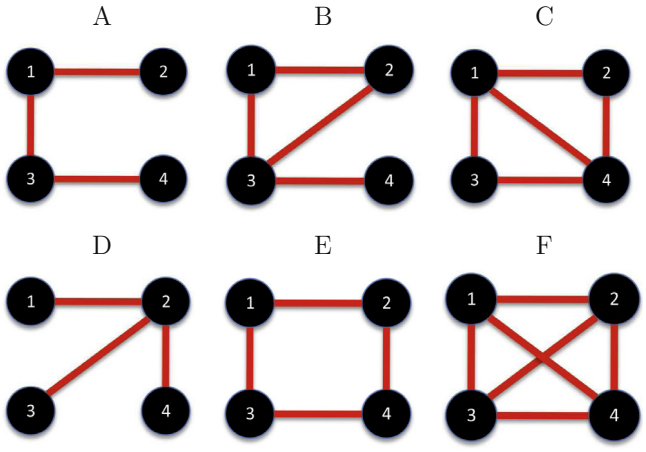

Fig. 1. The six different undirected subgraphs of size four, i.e., four connected vertices.

An important question in understanding the connection between structure and functionality of complex systems (e.g., neurological networks, cellular structure, food webs, electronic circuits, social networks) has been whether or not the structure of a given n-vertex subgraph can be referred to as a motif (Milo et al., 2002, 2004). Motifs are generally defined as recurring small connected subgraphs in a graph whose abundance is greater than would be expected compared to their abundance within an equivalent random graph (Milo et al., 2002, 2004). Knowledge and understanding of motifs is becoming important as they are basic functional building blocks combining and interacting to form larger-scale functions. For example, small-motifs within biological transcription networks been shown to be crucial to regulation of living cells (Mangan and Alon, 2003; Yeger-Lotem et al., 2004). Vázquez et al. (2004) have also demonstrated in cellular networks (i.e., transcription, metabolic, protein interaction) the abundance and aggregation of small subgraphs helps to define a network's large-scale organization. Since networks are constructed to summarize the structural or functional roles of an observed system, network subgraphs identified as motifs are thought to be important building blocks of the network and the system. For example, in a granular materials context, the closed three vertex subgraph, or triangle structure, can be identified as a motif in the contact network of a two-dimensional granular material. These triangles play an important structural and functional role in the physics of granular media (Tordesillas et al., 2010, 2012; Arévalo et al., 2010). In Milo et al. (2004), subgraphs can be identified as motifs by calculating a significance profile score, based on their prevalence in a given network, compared to their prevalence in a distribution of equivalent random networks.

As important as identifying whether a subgraph is a motif or not is the abundance ranking of the population of a subgraph in a network compared to other subgraphs in the same class. For example, for the six four vertex connected subgraphs whether one, or many, are technically motifs is not as relevant as whether one subgraph appears more frequently than another. Perhaps the best example of this is the superfamily phenomenon arising from the relative ranking of four vertex subgraphs in networks constructed from time series data. In Xu et al. (2008) it was shown that the rank-ordering of the population of four vertex subgraphs in so-called phase space networks could provide a broad classification of the underlying dynamical system responsible for the observed time series. That is, networks arising from chaotic time series data exhibited a different superfamily classification to networks arising from periodic time series data. The structure of each four vertex subgraph in these phase space networks also possess a physical interpretation of the geometry of reconstructed phase space and phase space trajectories. Moreover, this superfamily classification was also shown to be robust against moderate levels of observational noise on the time series (Xiang et al., 2012). For the networks we study here — structural contact networks of a granular material — *each of the six four vertex subgraphs have a physical and functional interpretation.* In two dimensions, only three of the subgraphs — those with cycles B, C and E — are technically motifs with respect to the significance profile score in Milo et al. (2004). The subgraph F — four triangles arranged in a three-dimensional tetrahedral-like configuration — arises less rarely in two-dimensional contact networks requiring a wide range of polydispersity to exist. We are thus interested in identifying the relative abundance, or

superfamilies, of the subgraphs in the contact networks of a wide range of granular assemblies. Of particular interest is to relate different superfamilies to the behavioral regimes or "phases" of the material throughout loading and to explore opportunities for merging the heretofore different perspectives adopted by the engineering and physics communities: i.e., pre-failure versus failure regimes (soil mechanics) or jammed versus unjammed regimes (physics). Ancillary to this is the extent to which topology governs these different regimes, given that this analysis solely focusses on the contacts between grains.

The remainder of this paper is organized as follows: in Section 2 we discuss the approach and methods used in our analysis. Section 3 provides a rundown of the superfamily phenomena observed in deforming dense granular materials. In Section 4 we discuss how generic the observed superfamily phenomena is with respect to geographically constrained random networks. We also shed some light on possible mechanisms within granular materials responsible for the observed superfamily phenomena. We also speculate on implications with respect to continuum modeling and the fabrication of tailor-made materials. Finally, in Section 5 we briefly summarize the main findings.

2. Methods

The geometrical arrangement of grains throughout loading tests can be usefully encoded in a complex network representation of the material (Walker and Tordesillas, 2010). A complex network or graph $G = (V, E)$ consists of vertices V and edges E. The set $E \subseteq V \times V$ and a member of E takes the form $e = (u, v)$ connecting vertices $u \in V$ and $v \in V$. The set of vertices in a contact network representation of a granular material consists of the grains and the set of edges summarizes the contact topology of the grains. That is, a network edge connects two vertices if the grains the vertices represent are in physical contact. An example of a contact network topology is displayed in Fig. 2. The contact network is an undirected and unweighted network and can conveniently be described by a symmetric binary adjacency matrix. In this case the vertices correspond to the rows and columns of the matrix and the edges are encoded by the non-zero elements of the matrix. It is possible to imbue the network, or adjacency matrix, with further information such as the contact force between contacting grains, and this leads to a weighted network. In the following we restrict our attention to the *undirected unweighted contact network* as it remains a challenge to reliably measure the forces at contacts in experimental tests of real granular materials.

A subgraph of a network $G = (V, E)$ is a graph $M = (V_m, E_m)$ where $V_m \subseteq V$ and the edges connecting members of V_m are such that $E_m \subseteq E$. The contact network of a granular assembly contains many subgraphs whose topologies alone provide functional relevance. For example, the subgraph consisting of three vertices with mutual connections, i.e., a 3-cycle or triangle topology, has important structural meaning within a granular assembly (Arévalo et al., 2010). The configuration of grains giving rise to network 3-cycles have the property of frustrating relative rotation among the grains so providing a stabilizing function (Tordesillas et al., 2011). These vertex triples have recently been identified to statistically determine the global structure of real-world complex networks (Jamakovic et al., 2009). A second subgraph within a granular material is one consisting of a connected chain of edges which, when imbued with knowledge of physical orientation and force carrying potential, can be interpreted as a force chain structure. Force chains are quasi-linear sequences of connected grains which possess load-bearing column-like functionality (Tordesillas, 2007).

In general network theory, small subgraphs consisting of a small number of vertices and their associated edges can be defined as motifs (Milo et al., 2004). These are subgraphs whose prevalence in the network (number of instances) is higher than would be expected in an equivalent random network (e.g., a randomly rewired — switched edges — version of the original network preserving the observed degree distribution). These special subgraphs are considered important because of their possible functional role (cf. the aforementioned 3-cycles). As Kashani et al. (2009) point out, the actual functional role some of these subgraphs might play can be unknown and only speculated at however, simply defining motifs based on topology and their prevalence is a good initial step in further understanding their function. Beyond the two connected triad subgraphs — an open and closed triangle — subgraphs consisting of four vertices and their connected edges are frequently studied. There are six possible connected subgraphs with four vertices in an undirected network as shown in Fig. 1. The frequency of these subgraphs in a network can be enumerated. See, for example,

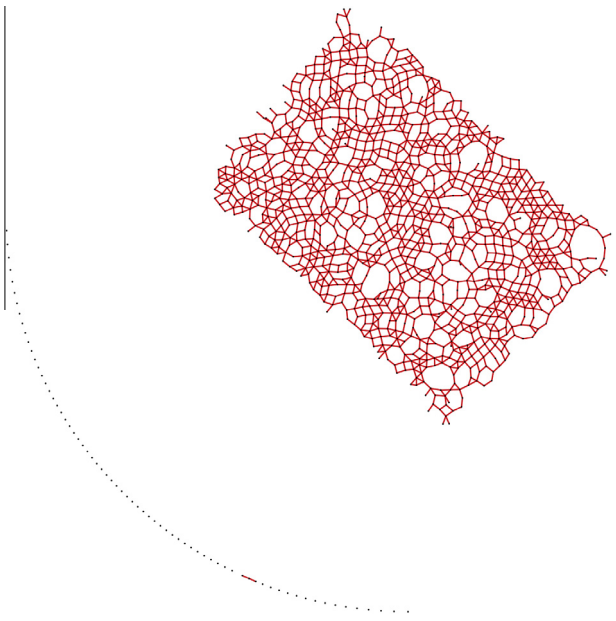

Fig. 2. Example of contact network topology arising in 2D photoelastic disk experiments The network is visualized using a Kamada–Kawai graph drawing style (Kamada and Kawai, 1989) implemented in R-igraph (Csardi and Nepusz, 2006). Isolated disks (rattlers) and small disconnected clusters are displayed around the largest connected component of disk contacts.

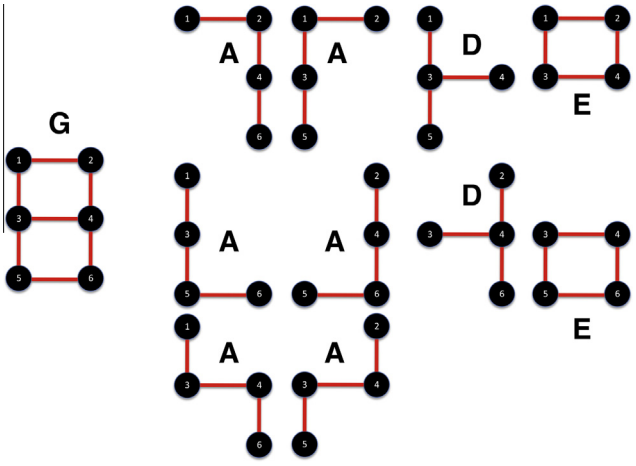

Fig. 3. An example network G and all of its four vertex subgraphs extracted: six A, two D and two E.

the algorithm of Kashani et al. (2009) which returns the number of instances or matches of each of Fig. 1 subgraphs in a network.

It is important to be aware that these matches allow overlap of vertices and edges (Kashani et al., 2009). For example, consider an arrangement of grains inducing the network G shown in Fig. 3. This graph could represent a larger granular structure consisting of two 4-cycles which share an edge and contains three different forms of the four vertex subgraphs A, D and E, with frequencies 6, 2 and 2 respectively. All of these subgraphs have been extracted, and we see that by searching for all matches of a given subgraph, we allow ourselves to appreciate the multitude of roles combinations of small subgraphs play in designing larger scale topologies. These motifs, or small connected subgraphs that permeate a graph, can thus be seen to be basic building blocks of complex networks. Observe that this interpretation of building block is more in line with layered sets of blueprints in architectural drawings, as opposed to jigsaw-style constructions suggested by the piecing together of the two 4-cycles in Fig. 3, or the set of minimal contact cycles (graph faces) in Fig. 2.

We are most interested in the relative ranking or the frequency of occurrence of each of these six subgraphs, as shown in Fig. 1, in the contact networks of a granular assembly throughout loading. That is, we are not overly concerned whether a particular subgraph is technically a motif, and more interested in the rank-order of the subgraphs into superfamilies. Recall, for a subgraph to be regarded as a network motif, its prevalence must be higher than expected when compared to an equivalent random network. Here, equivalence means the same number of vertices and identical degree distribution. For each contact network, we can generate such a random network by rewiring edges to preserve the local degree structure. The significance profile in Milo et al. (2004) can be used to detect if a given subgraph is a motif — a positive significant profile score above a specified threshold suggests a given structure is a network motif. We have tested this for the observed contact networks, and found that in two-dimensional contact networks subgraphs B, C and E, containing triangle topologies, can be typically regarded as motifs. However, in the present context, whether or not a subgraph is semantically a motif is ancillary to the superfamily ranking of each.

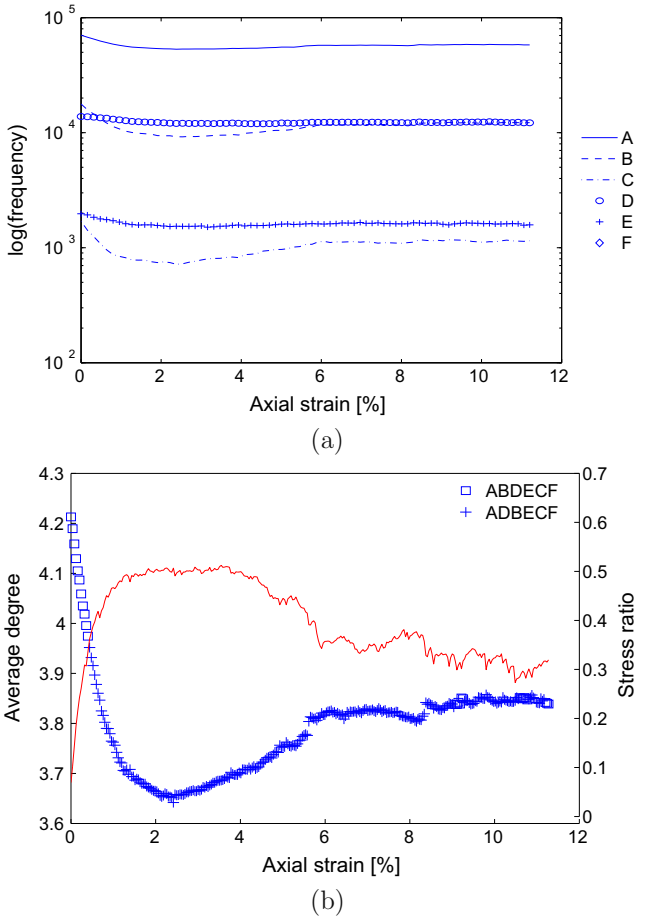

Fig. 4. (a) The observed frequency of the six subgraphs within the contact networks of 0.02CV. (b) The average degree of the contact networks plotted according to observed superfamily. The stress ratio indicating peak stress and onset of failure is also shown.

3. Results

In this paper we analyze simulated and experimental data from a number of disparate sources. In order to achieve some consistency in presentation, for each test we will display the observed frequency of subgraphs on a semi-log scale, and then present the observed superfamily with respect to the average contact network degree through loading. To aid interpretation of the average degree plots we include relevant information on the stress — stress ratio or deviator stress — evolution with respect to strain. For reasons that will become obvious, we depart slightly from this presentation style for the suite of photoelastic disk experiments.

In Figs. 4 and 5, we show the subgraph counts and corresponding superfamily classification through loading for the two two-dimensional biaxial compression simulations, subject to constant volume boundary conditions. We note that due to the narrow range of polydispersity, the subgraph F is not present, and so does not register on these log-scale plots. The DEM model used is designed to approximate the response of assemblies of noncircular particles by incorporating a moment transfer to account for rolling resistance (Oda and Iwashita, 2000). This adjustment to the classical DEM model of Cundall and Strack (1979) allows control of the relative rotations of particles at contacts. It has been found to be helpful in achieving more realistic rotations and stress predictions of systems with angular particles (e.g. Gutierrez and Mohamed, 2010). The two tests are distinguished by the coefficient of rolling friction. For convenience, we refer to these tests as 0.02 CV and 0.2 CV, where the number corresponds to the value of the coefficient of rolling friction μ^r, and CV to constant volume. Full details of the simulation and the DEM parameters can be found elsewhere (Tordesillas, 2007). The initial packing fraction for both tests was 0.858.

We see that there is no difference in the observed superfamilies with respect to the rolling friction model parameter. During the early stages of loading, and well before the axial strain value where peak stress ratio and failure occur, the observed superfamily is of the form ABDECF. As the average degree of the contact network falls below four for these two-dimensional tests, the superfamily classification changes to ADBECF and remains in this category for the remainder of the loading, including the onset and transition to failure. In the test with lower coefficient of rolling friction ($\mu^r = 0.02$ compared to $\mu^r = 0.2$), there are a few strain states when the superfamily switches back to the initial classification (see, Fig. 4(b)). This may in part be due to the shear band, which dominates dynamics after failure, temporally recovering integrity by forming large localized jammed areas. In the main, however, the observed superfamilies suggest that for a stable (early stages of strain-hardening when load can more easily be borne) granular material in two dimensions the contact network possesses the subgraph ranking ABDECF. As connectivity is lost as a result of grain rearrangements in response to increasing load, the material becomes more prone to failure and possesses the subgraph ranking

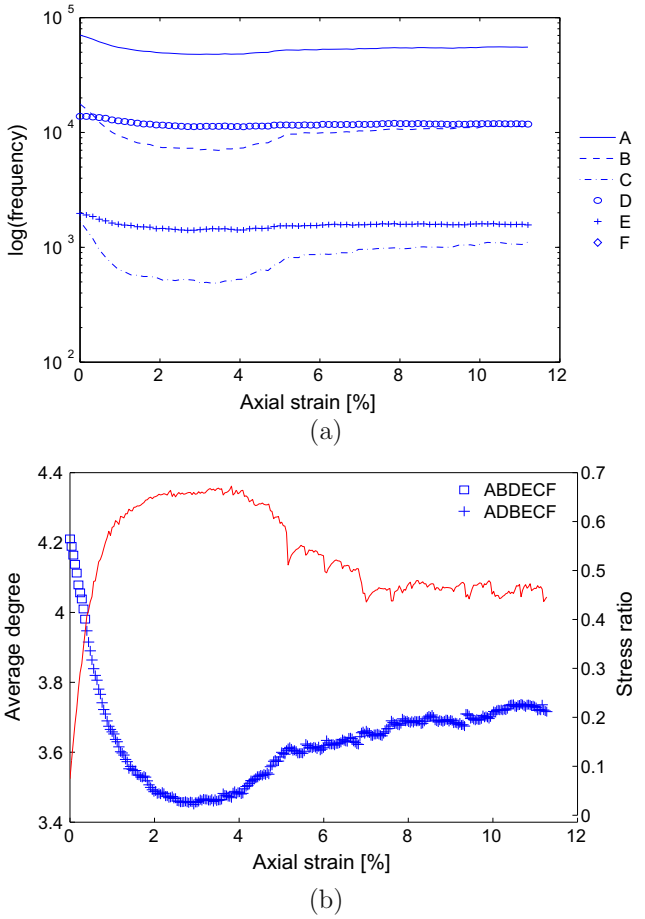

Fig. 5. (a) The observed frequency of the six subgraphs within the contact networks of 0.2CV. (b) The average degree of the contact networks plotted according to observed superfamily. The stress ratio indicating peak stress and onset of failure is also shown.

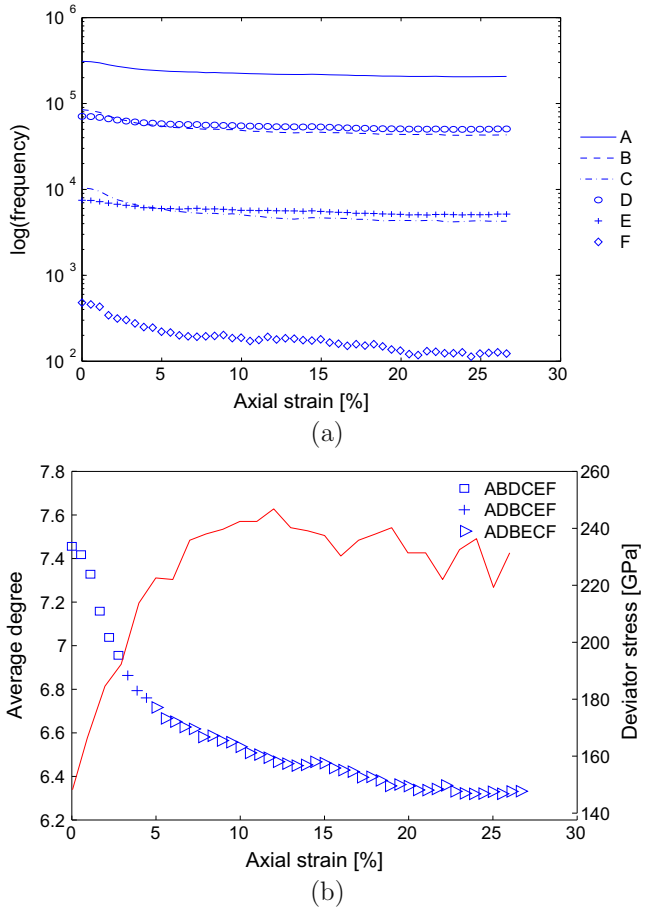

Fig. 6. (a) The observed frequency of the six subgraphs within the contact networks of the three-dimensional polyellipsoid test. (b) The average degree of the contact networks plotted according to observed superfamily. The change in deviator stress with respect to axial strain is also shown for this test system.

ADBECF. We note here, but will discuss in more detail later, that the important switch is from B to D. The B subgraph containing three particles with a fourth particle playing a supporting role by forming a triangle becomes less prevalent than the star-like subgraph D, which has no triangular support. We remark that we have also observed the same superfamily phenomena in two related two-dimensional biaxial compression tests subject to constant confining pressure boundary conditions (Tordesillas, 2007) (results not shown).

The three-dimensional compression simulation of polyellipsoid particles also fails in the presence of shear banding after reaching a peak stress (Peters et al., 2009). The initial porosity was 0.35. The subgraph counts are shown in Fig. 6. An effect of the extra dimension is readily apparent. The subgraph F, which corresponds to the basic three-dimensional building block tetrahedral structure, is now present. Its prevalence remains the lowest observed of the six subgraphs. We identify three different superfamilies for this three-dimensional test. Initially, we observe ABDCEF then ADBCEF before finally the sample exhibits the ADBECF superfamily. That is, there are two transitions in subgraph abundance: B loses out to D and then C loses out to E. Both transitions occur before peak stress and failure in this system. Compared to the two-dimensional simulation, there is a difference in the initial superfamily and the existence of the second transition involving the subgraphs C and E. We will discuss these subgraphs in more detail later, but make two observations. The transition causing E to become higher ranked than C again involves the loss of a triangle topology, actually, the loss of two triangles. The topologies and transitions between subgraphs C and E are reminiscent of the T1 transition in foams (Weaire et al., 2007), as well as the postulated shear transition zone (STZ) mechanism of failure (Mesarovic et al., 2012). In this latter case, however, with respect to subgraph counts this transition is secondary to the change in the ranking of subgraphs B and D.

Once again, we see that when the material is more stable, the superfamily ranks B above D, whereas the more prone to failure state of the contact network exhibits the superfamily ADBECF. We have also discovered the same superfamily in two other three-dimensional tests which are specifically set up to fail. The diffuse failure simulation studies of Sibille et al. (2009) exhibit the ADBECF superfamily once perturbation begins around peak stress. That is, the switch from the stable superfamily has already occurred, and subsequent perturbations towards diffuse failure do not change the superfamily. Similarly, the shear simulations of Sun et al. (2013) specifically designed to study shear banding consistently manifests the ADBECF superfamily.

The three-dimensional experimental systems we examine are triaxial compression tests. As was the case for the two-dimensional and three-dimensional simulations these experimental tests fail in the presence of a persistent shear band, i.e., the failure mode is also strain localization (Andò et al., 2013). There are two major differences between these experimental tests and the simulations, the obvious being that the simulations are only models, whereas the experiments are real. However, being experiments, they suffer

observational error, which in the present context corresponds to over-counting or under-counting of contacts. However, the resolution and capability is remarkable and as demonstrated in Andò et al. (2013), enough information is recorded to recover essential features of the triaxial compression process. The second major difference is the scale of the systems. The number of grains within the simulations presented in detail above exceed ∼5000. In the triaxial sand tests, the number of observed grains is much greater. In the Caicos ooid sample there are initially ∼84,000 grains, and in the Hostun sand sample ∼54,000 grains. The initial porosity for the Caicos ooid sample was 35.2%, and for the Hostun sample the initial porosity was 39.7%. In the interest of a more direct comparison between the simulations and these experiments, and also to avoid some noise in the X-ray images for grains at the boundaries, we extract a central core of observations in each sample to study. This results in the Caicos ooid sample core containing ∼15,000 grains with ∼8000 grains in the Hostun sand sample. We have tested the full sets of assemblies, but noise in the full imaging measurements for Hostun creates enough spurious contacts to bias results. These observational noise issues were less damaging for the Ottawa sand test sample, and so we use the entire sample of ∼27,000 grains. The initial density of the Ottawa sample was 1.73 g/cm^3.

The results of the subgraph analysis for the cores of the Caicos ooid and Hostun sand tests are shown in Figs. 7 and 8, respectively. As for the three-dimensional simulation, we see that the tetrahedral building block structure registers a presence, but is still ranked

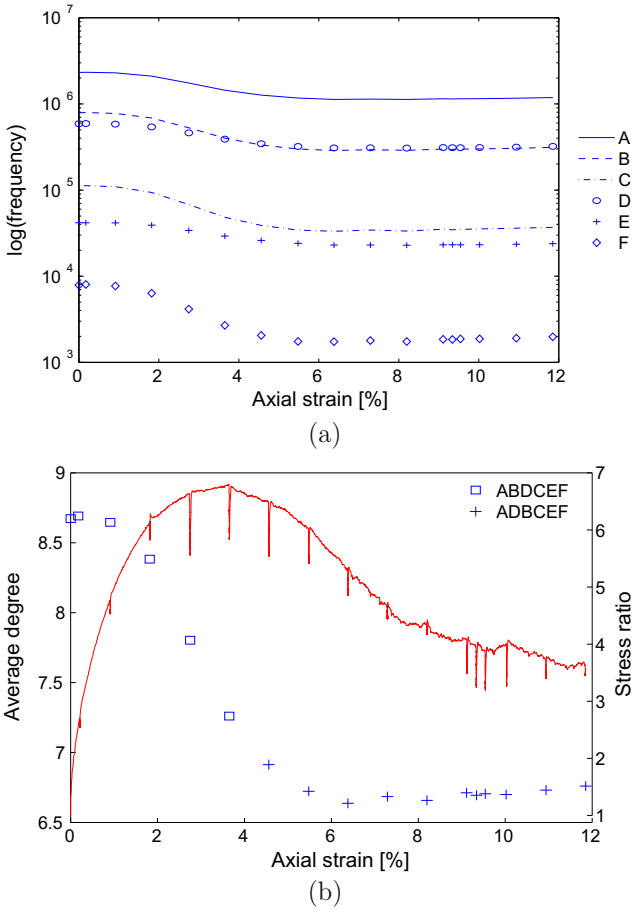

Fig. 7. (a) The observed frequency of the six subgraphs within the contact networks of Caicos ooid. (b) The average degree of the contact networks plotted according to observed superfamily. The stress ratio is also shown to indicate peak and the onset of failure.

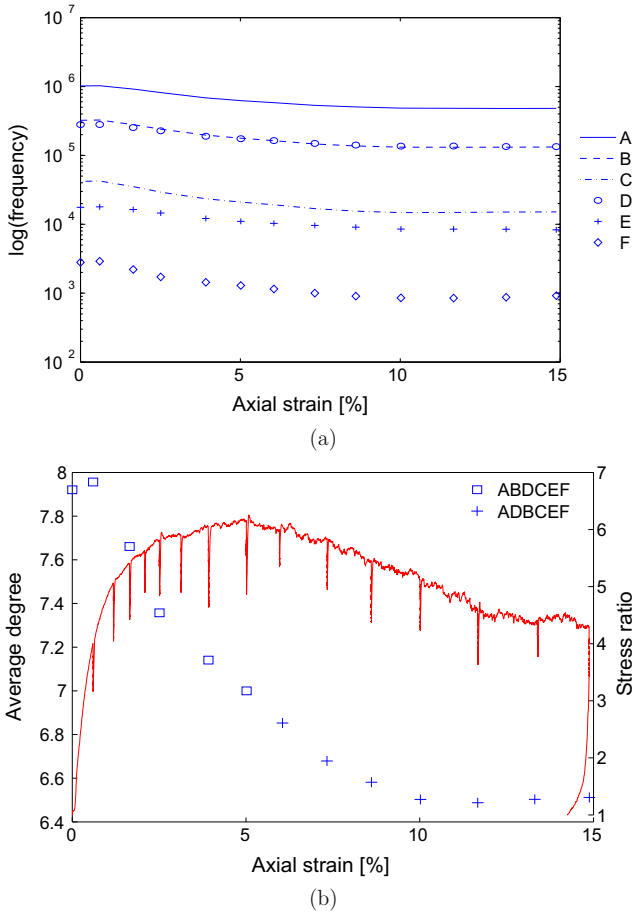

Fig. 8. (a) The observed frequency of the six subgraphs within the contact networks of Hostun. (b) The average degree of the contact networks plotted according to observed superfamily. The stress ratio indicating peak stress and onset of failure is shown.

the lowest. The evolution of its frequency for the Caicos ooid test is interesting, with almost an order of magnitude drop in occurrence in the lead up to failure. The transition in superfamily from the more stable ABDCEF to the more failure-prone ADBCEF occurs. Unlike the three-dimensional simulation, we do not observe the second T1-like transition of subgraph C ceding prominence to subgraph E. However, the observed counts suggest that the population of these two structures are becoming comparable. For the Ottawa sand test sample, as shown in Fig. 9, we see the same superfamily as observed in the three-dimensional simulation of polyellipsoid particles. That is, ABDCEF transitions to ADBCEF and then to ADBECF before and during the point of failure. (Note the initial configuration, or the first observed state of deformation is actually ADBCEF before the onset of compression closes some dilatant holes in the sample.)

Overall, we observe first the change in superfamily ABDCEF to ADBCEF and then to ADBECF appears to be universal across two-dimensional, three-dimensional, simulated and real sand tests. The dominant transition is the switch in prominence of the B and D subgraphs with a lesser role being played by the C to E switch. This suggests there may well be an underlying universal dynamical law of granular materials during the transition to failure responsible for this universality in structural self-organizational properties. Of course, we are merely counting the prevalence of such structures, and inferring possible transitions. A more thorough analysis on transition dynamics would perhaps employ the techniques used in Tordesillas et al. (2012). We reserve this for a future study.

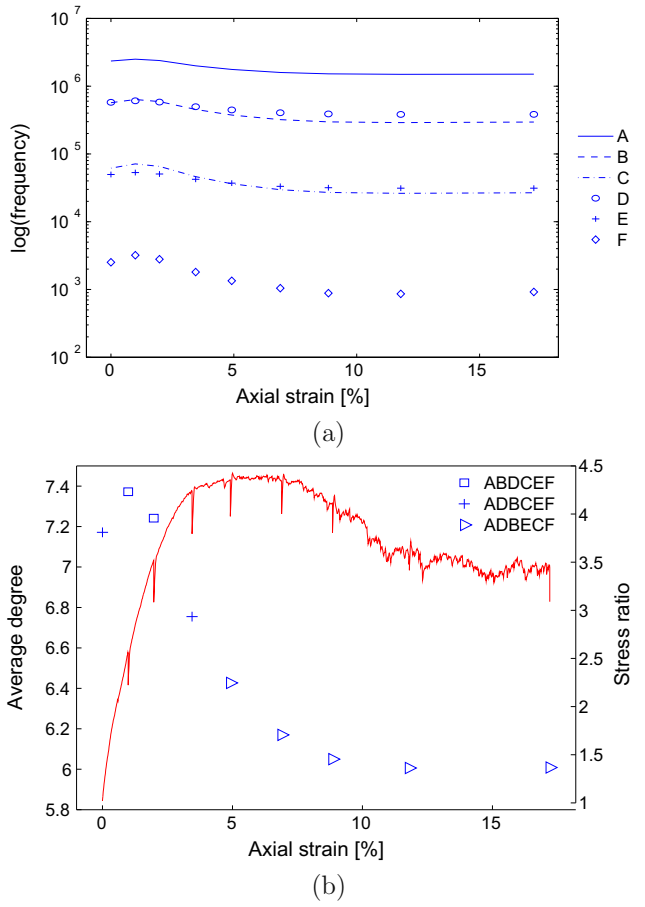

Fig. 9. (a) The observed frequency of the six subgraphs within the contact networks of the Ottawa sand sample. (b) The average degree of the contact networks plotted according to observed superfamily. Stress–strain information is also shown indicating where contacts were observed during the deformation.

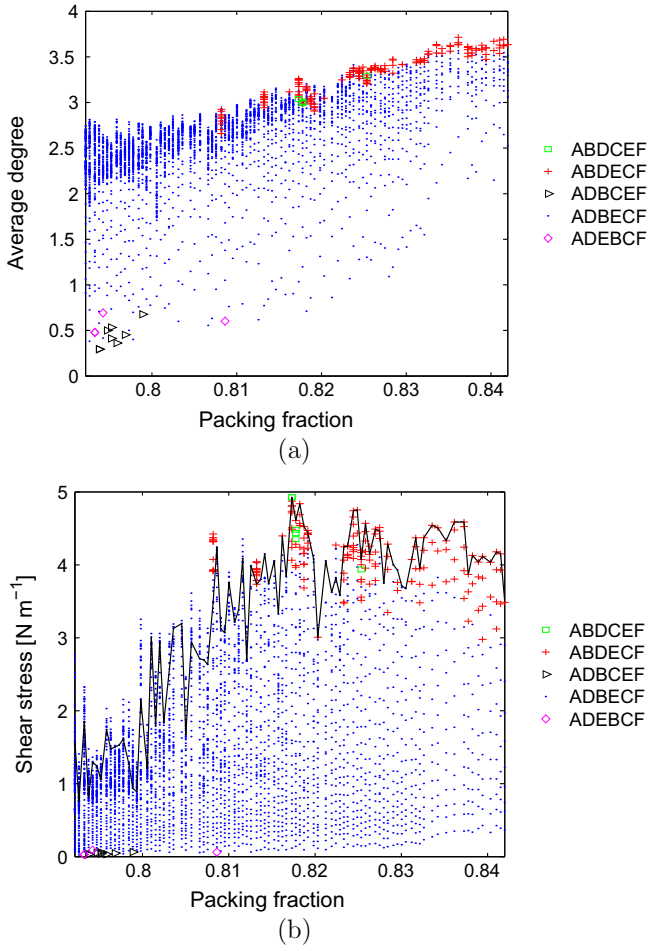

Fig. 10. Photoelastic disk shear packing fraction test and superfamily phase diagram (a) plotted with respect to average degree, (b) plotted with respect to shear stress for comparison with Fig. 2(c) in Bi et al. (2011). The black line indicates the shear stress of the assemblies at the final observed shear step in each packing fraction test.

The superfamily classification and its changes within frictional granular systems in response to loading suggests a connection to the jamming concept of Liu and Nagel (1998) where, depending on density, a material is unjammed — can flow under applied stresses — or jammed — can resist small stresses. Bi et al. (2011) explored this framework with respect to frictional granular particles — photoelastic disks — and proposed a modification to the jamming phase diagram. Bi et al. (2011) exploited the properties of photoelastic materials to infer contact forces and introduced two new states for frictional granular systems: fragile and shear-jammed. Their experiments were two-dimensional and the fragile state occurs when the so-called strong network percolates in only one direction. The system is classified as shear-jammed if the strong network percolates in both dimensions. We are interested in how the superfamily concept on contact networks, as introduced here, compares to the proposed jamming diagram of Bi et al. (2011). We use a subset of the data sets used in Bi et al. (2011) but only consider the topological contact network. That is, we do not consider contact force information in our framework. As a result we expect differences to arise, but it is informative to see how much the superfamily classification solely based on topology provides.

In Fig. 10(a) we plot each of the 90 tests with respect to the initial packing fraction and the observed average degree of the contact network through shearing. The symbols used identify the superfamily classification in the legend. There are five observed superfamilies. Two appear to be pathological cases ADEBCF (diamonds) and ADBCEF (triangles) which occur at low packing fractions when the assembly is loose, resulting in a fragmented contact topology where each connected component has very few contact edges. The dominant superfamily is the one we term failure-prone ADBECF (dots) and this encompasses most of the tests. This also covers the entire fragile state and the lower part of the shear-jammed state in the phase diagram of Bi et al. (2011) (Fig. 2(c) of their paper). As the average degree rises to above three (minimum degree, or coordination number required for isostatic conditions), the observed superfamily transitions to the more stable family ABDECF (crosses). This superfamily occurs within the shear-jammed zone of the Bi et al. (2011) jamming diagram as does the rarely observed ABDCEF (squares) superfamily. This superfamily is the one observed at the start of loading in the three-dimensional tests explored above.

In Fig. 10(b), we plot the superfamily classification with respect to shear stress, allowing a more direct comparison with the results of Bi et al. (2011). We see that our superfamily phase diagram is qualitatively similar to the jamming diagram in Bi et al. (2011), showing that classification through topology alone is a good coarse-grain description of a system. The superfamily classification without force information widens the number of systems that can be classified. Furthermore, by not relying on percolation of strong forces between well-defined system domain boundaries, a greater number of engineering tests with more exotic domain boundaries can also be absorbed in our framework.

We have seen, using solely topology, that qualitative features of the Bi et al. (2011) proposed jamming phase diagram can be recovered using our proposed superfamily classification. However, the proposed fragile state did not emerge in Fig. 10(b). An extension of the methods is thus required to uncover this state. Such an extension would be to extend the superfamily classification to force-weighted networks. Force-weighted networks have been shown recently to be useful for analyzing the effects of network topology to acoustic propagation in granular materials (Bassett et al., 2012), and network communities within force-weighted networks can be closely linked to force chains (Bassett et al., 2014). In the first instance, an extension of the present superfamily work to force-weighted networks would involve thresholding the contact network according to observed contact force magnitude. For example, we could consider the filtered subnetwork of contacts that bear above-average force. Then we could classify the superfamily of subgraph structures. Such an approach could, potentially, uncover the other proposed states in the Bi et al. (2011) jamming phase diagram. We reserve this approach for a later paper as it would only be applicable to tests where contact force can be reliably measured.

4. Discussion

4.1. Random networks

Motifs, defined as recurring small connected subgraphs in a graph, comprise the basic building blocks of a complex network (Jamakovic et al., 2009). Their frequencies of occurrence can also be related to their different functional roles in the system the network represents (Milo et al., 2002). The contact network can be regarded as a geographical complex network, since the grains themselves can block potential (abstract) contacts between other neighboring grains. One might ask if the observed superfamilies in granular contact networks can be solely attributed to these geographical constraints on the topology. We undertook a series of basic randomization tests to discover if a random network subject to geographical constraints exhibits different superfamily phenomena.

We generated random geographical networks in both two and three dimensions. The procedure in each dimension was essentially the same. For a given number of points (to be regarded as grain centres) we randomly (uniformly distributed in each direction) placed them in the unit square or cube. To generate contacts, we performed a Delaunay triangulation on these points. Thus, in two dimensions a network of triangles was created corresponding to a tightly packed polydisperse system. The polydispersity depended on the initial spatial distribution of the randomly placed points and the geographical nature of contact networks was somewhat respected. Of course, edges along the convex hull of the points lead to unrealistic long-range contact network connections, but compared to the interior of the sample these were few in number. Irrespective of this potential bias, the goal of this first-step analysis is not to generate a random realizable contact network, only a random network with some geographical constraints. Generating a realizable random contact network in general is undoubtably a more challenging problem, and perhaps the methods of Small et al. (2014, submitted for publication) with specific constraints may be usefully employed. For example, two constraints could be to preserve the number of contacts of a packing and also to preserve the density of contacts in the packing. From a networks perspective this may be achieved by matching degree distributions and nearest neighbor degree distributions. Alternatively, the lattice-based random geometric network construction of Itzkovitz and Alon (2005), with suitable constraints may also be employed. In three dimensions, our construction of random networks follows the two-dimensional construction above, except for the initial "fully" connected networks being made up of tetrahedral structures.

For each initial random network — 100 in total — we randomly delete edges at a specified probability. For each probability, we perform the random attack 100 times to generate 100 networks. That is, all the edges in the initial network are attacked with the given probability to produce a less-connected network. This process is repeated 100 times to obtain for each probability 100 geographically constrained networks. The edge removal is random, so this analysis is again only a first-step to examining the universality of the superfamily phenomena. The random process should in no way be considered as the mechanism whereby a granular system loses contacts.

The results of these randomization tests for the two-dimensional and three-dimensional cases are shown in Fig. 11. The results are shown for initial networks with 5000 points/nodes but networks with fewer and greater number of nodes have been tested and the results appear robust. In each case we observe a first-order phase transition at connectivity probability 0.4 with respect to superfamily classification. A similar transition in superfamily phenomena was observed by Zhang et al. (2013) in their exploration of preferential attachment methods for randomly generating scale-free complex networks. When the probability of edge removal is low, the dominant superfamily in both cases is ABDCEF, which is the stable superfamily seen in the initial preparations of the three-dimensional systems. After the phase transition, and at lower connectivities (higher edge removal probability), we observe

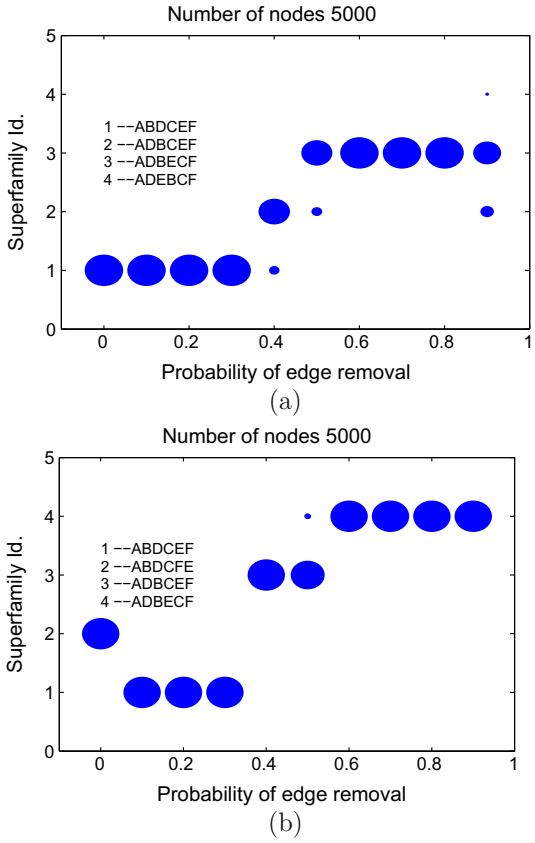

Fig. 11. Observed superfamilies in geographically constrained random networks in (a) two dimensions (b) three dimensions. "Delaunay network" edges are attacked randomly at a given probability and the superfamily of the resulting network is recorded. At each probability 100 networks are realized and the frequency of the observed superfamily corresponds to the displayed circle size.

the superfamily ADBECF. This is precisely the failure-prone superfamily we observe in all of the granular tests. The superfamily at the transition point is ADBCEF, observed as the intermediate state in the three-dimensional polyellipsoid simulation and the Ottawa sand test, as well as the final state of the Caicos ooid and Hostun sand tests. The initial preparation of the two-dimensional biaxial compression test does not feature in these random tests. Furthermore, we see that the initial networks in the three-dimensional random tests show a pathological case with a high ranking of subgraph F topologies, which can be attributed to the "Delaunay network" construction.

These first-step randomization tests suggest that the geographical constraints on topology for contact networks of a given connectivity strongly determines the superfamily. Thus, contact networks appear to be but one class of physical examples of, perhaps, a generic property of such geographical networks. This universality might be regarded as disappointing in the sense that there is nothing special about granular contact networks from a topological classification perspective. However, what is special is knowledge of the precise mechanisms governing grain rearrangements causing the transition from the "stable" superfamily to the "failure-prone" superfamily. We may end up with the same superfamily as random deletion of network edges, but a different process is clearly taking us there (cf. strain localization). To uncover possible mechanisms behind the transition, we try to give a (granular) physical interpretation to each subgraph structure.

4.2. Mechanisms

In the contact network representation, the abstract subgraphs in Fig. 1 can also have a direct physical interpretation, as they correspond to structural arrangements of grains. We conjecture that the relative abundance and superfamily classification of these structures helps to identify, and can be used to propose, the preferred design principles employed in the self-organization of a granular material in response to load in order to aid its load-bearing capabilities. The following individual interpretations with respect to grain clusters and other materials can be attributed to the six subgraphs shown in Fig. 1.

A: this configuration is the most basic of the four vertex connected subgraphs consisting of three connected line segments, corresponding to a chain of four particles. Force chains consist of three or more contiguous particles in a (physical) quasi-linear arrangement (Tordesillas, 2007). Note the network representation does not account for the physical orientation of the contact, and so the quasi-linear arrangement of grains required of a functional force chain is not enforced. Thus this configuration provides only a (very) conservative upper bound for the number of force chains of length 4.

B: this subgraph consists of a triangle, or 3-cycle topology, plus one extra edge. It could also be regarded as a length 3 force chain supported by a weak particle in the form of a triangular topology. Triangle contact topologies (in two dimensions) are the most stable of configurations particles in an assembly can form (Tordesillas et al., 2011). An assembly with a higher propensity of these structures compared to another assembly suggests a zeroth-order ranking in terms of stability or mechanical rigidity.

C: this structure consisting of two triangle contact topologies sharing a contact suggests even greater stability than subgraph B. Furthermore, this arrangement of contacts can be interpreted as a configuration that typifies an idealized T1 process observed and theorized in foams (Weaire et al., 2007). These topologies could also indicate the initial state of a local rearrangement contributing to microbanding (Tordesillas et al., 2008; Kuhn, 1999) or STZ (Mesarovic et al., 2012). The abundance, or lack thereof, of these topologies in the contact network gives an indication of the likelihood of such events occurring and being responsible for the dissipation of energy and failure within sheared materials.

D: this conformation is acyclic being in a star formation. Within the contact network this topology suggests that, at the larger mesoscale level, the central vertex is the nexus of adjacent larger n-cycles ($n > 3$), i.e., more likely to be present in zones of the material with high dilatancy. This subgraph can also be formed by the subgraph B losing its triangle but otherwise retaining all other contacts. This suggests a basic mechanism in the failure by buckling of a model force chain: subgraph B transitions to subgraph D.

E: this cluster arrangement, in common with 3-cycle or triangle topologies, is one of the building blocks of a granular material. In contrast to triangles this 4-cycle contact topology allows for relative non-frustrated rotations — roller bearing-like — amongst the constituent particles. Furthermore, this configuration can also be identified as an intermediate stage in an idealized T1 process.

F: in three dimensions this topology is a representation of the most basic tetrahedral configuration. In the systems we have studied, the superfamily ranking of this subgraph is always the lowest. However, examining its abundance through deformation, we see these structures decreasing in population prior to failure. It is reasonable to expect that these tetrahedral configurations occur in more densely packed areas of a sample where force chains are more likely to proliferate. The fall in abundance of these structures is thus indicative of dilation and a reduction in support to force chains, and perhaps their failure. Since this subgraph consists of four 3-cycles, our interpretation regarding the functionality of subgraph B and the transition BD → DB is also consistent with respect to subgraph F. That is, our conjectured mechanism for failure is transportable from two dimensions to three dimensions.

In all of the simulation and experimental compression tests, a distinguishing feature of the change in superfamily from stability to failure-prone is the configuration associated with dilatancy (subgraph D) — ranked only second to the basic chain configuration; A — switches its place in the superfamily with configuration

B. That is, configuration B loses a 3-cycle and becomes configuration D. Thus, as mentioned above, if one wishes to develop a continuum model within a formalism which scales-up from the mesoscale, the B to D transition mechanism should be incorporated from the get-go.

Of equal or more significance is the place in the superfamilies of the subgraph configuration C, which represents an idealized initial or final state of a T1 transition. This is of note because, despite these being promoted as ideal configurations and transitions, to explain the micromechanics of dilatancy and onset of failure in granular materials (Mesarovic et al., 2012), with respect to the superfamily classification, C to E in prevalence is a secondary transition. The transition of C to E does involve the dilatant change associated with loss of 3-cycles, and so perhaps a more representative initial mesoscale configuration should also include this topology. That is, the continuum formalism should scale-up from an initial force chain supported by weak particles encompassing both subgraph B and subgraph C topologies. Thus, the failure mechanism to be modeled would then incorporate the dilatant B to D and C to E mechanisms, thus capturing both force chain buckling and STZ topological transitions.

4.3. Tailor-made materials

The superfamily classification corresponding to stable topological arrangements (ABDCEF) and failure-prone arrangements (ADBECF) suggests a simple test for tailor-made fabricated materials. If the design requires a stable topology, then build a structure exhibiting the ABDCEF superfamily. Of course, if materials and design allows, one might want to shift the ranking of subgraph F to be as high as possible. For example, the three-dimensional Delaunay triangulation induces a network with the superfamily ABDCFE. On the flip-side, perhaps short term stability, or built-in obsolescence, is desirable; therefore, incorporating built-in fragility along the lines of the ADBECF superfamily should be considered.

5. Conclusion

The structural arrangement of grains in an assembly can be represented by a complex network. This representation provides a useful framework to study the material at multiple scales. Global network averages of local vertex properties gives a macroscopic description, whereas individual vertex properties reside at the microscopic or grain-scale. The global network quantity of average degree, closely related to a materials coordination number, is very useful for the characterization of a material. However, beyond knowledge of average loss or gain of contacts during deformation, the average degree does not provide detail on what grain rearrangement mechanisms may be responsible for the change in contacts. To help uncover such mechanisms, in this paper, we have considered the assembly and representative network at a larger mesoscopic scale by examining small subgraphs consisting of four connected vertices. We select four vertex subgraphs for two reasons (1) algorithms exist to enumerate all such subgraphs in a network, and (2) the evolution of both 3-cycle triangular, and 4-cycle square, topologies are encapsulated by the four vertex subgraphs. Moreover, one of the subgraphs, denoted F, is a direct representation of a three-dimensional structure, i.e., the tetrahedra. By examining the changing population of these four vertex subgraphs, e.g., subgraphs with triangles switch abundance with square subgraphs, we gain knowledge of dilatory mechanisms beyond a change in degree. Small subgraphs in a network are considered to provide important functional roles for the system they represent. Motifs which are a subset of these subgraphs that appear more often than expected are regarded as particularly important. Equally important is the relative frequency in a network of all subgraphs of a given size, with rank-orders of subgraphs exhibiting superfamily phenomena. We have found that the rank-ordering of four vertex subgraphs in contact networks of sheared granular assemblies also exhibit superfamily phenomena. There appears to be a universal superfamily (ADBECF) associated with the failure regime of granular assemblies irrespective of dimension or loading condition. Furthermore, the transition to this failure-prone superfamily involves the change in ranking of the subgraphs B to D, i.e., in moving from stable response to failure response, the prevalence of subgraph D surpasses subgraph B. The fall in abundance of subgraph B — a topology that contains a sTable 3-cycle arrangement — to below the frequency of subgraph D — a topology with no low order cycles — is indicative of the inherent dilatant grain rearrangements associated with failure mechanisms. For example, the transition in superfamily ranking of BD → DB could be regarded as the fundamental mechanism underlying force chain buckling. Moreover, the relatively low ranking of subgraphs C and E, and their superfamily transition CE → EC, corresponding to idealized T1 transition in foams hints at the possibility of a wider application and discovery of superfamily behavior to other materials. The qualitative features of the jamming phase diagram could also be captured through our proposed superfamily framework, as are prevalent or dominant fabric domains in the pre-failure versus failure regimes. Thus the superfamily phase diagram provides the possibility of bridging the gap between idealized physics experiments and soil mechanics tests. The suggestive universality of our results warrants further investigation to include more experiments on assemblies of real sand. As Matsushima and Blumenfeld (2014) remark, key to progress in identifying relationships between physical properties and properties of grain-packings is to identify emergent structures that are independent of many material properties. Here, across a number of different tests, comprising different materials, real and simulated, we have seen such independence and possible universality of the structural superfamily classification.

Acknowledgments

This work was partially supported by US Army Research Office (W911NF-11-1-0175, W911NF-1-11-0110), the Australian Research Council (DP120104759), NSF grants (NSF-DMR1206351, NSF-DMS1248071), NASA-NNX10AU01G and the Melbourne Energy Institute. AD, KA and AT thanks the US National Science Foundation and the Australian Academy of Science for support. We thank Mark Hopkins, Matthew Kuhn and Luc Sibille for kindly making data from their DEM simulations available for study. We thank the anonymous referees for helpful suggestions to improve the presentation of this manuscript.

References

Andò, E., Viggiani, G., Hall, S.A., Desrues, J., 2013. Experimental micro-mechanics of granular media studied by x-ray tomography: recent results and challenges. Géotech. Lett. 3, 142–146.

Arévalo, R., Zuriguel, I., Maza, D., 2010. Topology of the force network in the jamming transition of an isotropically compressed granular packing. Phys. Rev. E 81, 041302.

Bassett, D.S., Owens, E.T., Daniels, K.E., Porter, M.A., 2012. Influence of network topology on sound propagation in granular materials. Phys. Rev. E 86, 041306.

Bassett, D.S., Owens, E.T., Porter, M.A., Manning, M.L., Daniels, K.E., 2014. Extraction of force-chain network architecture in granular materials using community detection. Available from: <arXiv:1408:3841v1[cond-mat.soft]>.

Bi, D., Zhang, J., Chakraborty, B., Behringer, R.P., 2011. Jamming by shear. Nature 480, 355–358.

Csardi, G., Nepusz, T., 2006. The igraph software package for complex network research. InterJournal Complex System, 1695 <http://igraph.sf.net>.

Cundall, P.A., Strack, O.D.L., 1979. A discrete numerical model for granular assemblies. Géotechnique 29, 47–65.

Druckrey, A.M., Alshibli, K.A., 2014. 3D behavior of sand particles using X-ray synchrotron micro-tomograph. In: Geo-Congress 2014 Technical Papers, pp. 2814–2821, doi: http://dx.doi.org/10.1061/9780784413272.272.

Gutierrez, M., Mohamed, A., 2010. Comprehensive DEM study of the effects of rolling resistance on strain localization in granular materials. Granular Matter 12, 527–541.

Itzkovitz, S., Alon, U., 2005. Subgraphs and network motifs in geometric networks. Phys. Rev. E 71, 026117.

Jamakovic, A., Mahadevan, P., Vahdat, A., Boguñá, M., Krioukov, D., 2009. How small are building blocks of complex networks. Available from: <arXiv:0908.1143v1[physics.soc.ph]>.

Kamada, T., Kawai, S., 1989. An algorithm for drawing general undirected graphs. Inform. Process. Lett. 31, 7–15.

Kashani, Z.R.M., Ahrabian, H., Elahi, E., Nowzari-Dalini, A., Ansari, E.S., Asadi, S., Mohammadi, S., Schreiber, F., Masoudi-Nejad, A., 2009. Kavosh: a new algorithm for finding network motifs. BMC Bioinf. 10, 318.

Kuhn, M.R., 1999. Structured deformation in granular materials. Mech. Mater. 31, 407–429.

Liu, A.J., Nagel, S.R., 1998. Jamming is not just cool anymore. Nature 396, 21–22.

Mangan, S., Alon, U., 2003. Structure and function of the feed-forward loop network motif. PNAS 100, 11980–11985.

Matsushima, T., Blumenfeld, R., 2014. Universal structural characteristics of planar granular packs. Phys. Rev. Lett. 112, 098003.

Mesarovic, S.D., Padbidri, J.M., Muhunthan, B., 2012. Micromechanics of dilatancy and critical state in granular matter. Géotech. Lett. 2, 61–66.

Milo, R., Shen-Orr, S., Itzkovitz, S., Kashtan, N., Chklovskii, D., Alon, U., 2002. Network motifs: simple building blocks of complex networks. Science 298 (5594), 824–827.

Milo, R., Itzkovitz, S., Kashtan, N., Levitt, R., Shen-Orr, S., Ayzenshtat, I., Sheffer, M., Alon, U., 2004. Superfamilies of evolved and designed networks. Science 303, 1538–1542.

Oda, M., Iwashita, K., 2000. Study on couple stress and shear band development in granular media based on numerical analysis. Int. J. Eng. Sci. 38, 1713–1740.

Peters, J.F., Hopkins, M.A., Kala, R., Wahl, R.E., 2009. A poly-ellipsoid particle for non-spherical discrete element method. Eng. Comput. 26, 645–657.

Russell, S., Walker, D.M., Tordesillas, A., submitted for publication. Optimized flows and pore connectivity in the presence of shear bands: a characterization of the coupled evolution of grain fabric and pore space using complex networks. J. Mech. Phys. Solids.

Sibille, L., Nicot, F., Donzé, F.V., Darve, F., 2009. Analysis of failure occurence from direct simulations. Eur. J. Environ. Civil Eng. 13, 187–201.

Small, M., Hou, L., Zhang, L., 2014. Random complex networks. Natl. Sci. Rev. http://dx.doi.org/10.1093/nsr/nwu021.

Small, M., Stemler, T., Judd, K., submitted for publication. Super-star networks: growing optimal scale-free networks via likelihood. Phys. Rev. Lett.

Sun, W.C., Kuhn, M.R., Rudnicki, J.W., 2013. A multiscale DEM-LBM analysis on permeability evolutions inside a dilatant shear band. Acta Geotech. 8, 465–480.

Tordesillas, A., 2007. Force chain buckling, unjamming transitions and shear banding in dense granular assemblies. Philos. Mag. 87, 4987–5016.

Tordesillas, A., Muthuswamy, M., Walsh, S.D.C., 2008. Mesoscale measures of nonaffine deformation in dense granular assemblies. J. Eng. Mech. – ASCE 134, 1095–1113.

Tordesillas, A., Walker, D.M., Lin, Q., 2010. Force cycles and force chains. Phys. Rev. E 81, 011302.

Tordesillas, A., Lin, Q., Zhang, J., Behringer, R.P., Shi, J., 2011. Structural stability and jamming of self-organized cluster conformations in dense granular materials. J. Mech. Phys. Solids 59, 265–296.

Tordesillas, A., Walker, D.M., Zhang, J., Behringer, R.P., 2012. Transition dynamics and magic-number-like behavior of frictional granular clusters. Phys. Rev. E 86, 011306.

Tordesillas, A., Walker, D.M., Andò, E., Viggiani, G., 2013. Revisiting localized deformation in sand with complex systems. Proc. R. Soc. A 469, 201220606.

Vázquez, A., Dobrin, R., Sergi, D., Eckmann, J.-P., Oltvai, Z.N., Barabási, A.-L., 2004. The topological relationship between the large-scale attributes and local interaction patterns of complex networks. PNAS 101, 17940–17945.

Walker, D.M., Tordesillas, A., 2010. Topological evolution in dense granular materials: a complex networks perspective. Int. J. Solids Struct. 47, 624–639.

Weaire, D., Vaz, M.F., Teixeira, P.I.C., Fortes, M.A., 2007. Instabilities in liquid foams. Soft Matter 3, 47–57.

Xiang, R., Zhang, J., ke Xu, X., Small, M., 2012. Multiscale characterization of recurrence-based phase space networks constructed from time series. CHAOS 22, 013107.

Xu, X., Zhang, J., Small, M., 2008. Superfamily phenomena and motifs of networks induced from time series. PNAS 105, 19601–19605.

Yeger-Lotem, E., Sattah, S., Kashtan, N., Ikzkovitz, S., Milo, R., Pinter, R.Y., Alon, U., 2004. Network motifs in integrated cellular networks of transcription-regulation and protein-protein interaction. PNAS 101, 5934–5939.

Zhang, L., Small, M., Judd, K., 2013. Exactly scale-free networks. Available from: <arXiv:1309.0961v3[physics.soc.ph]>.